2-1-2021

Fronto-cerebellar connectivity mediating cognitive processing speed

Clive H Y Wong

Jiao Liu

Tatia M C Lee

Jing Tao

Alex W K Wong

See next page for additional authors

Authors

Clive H Y Wong, Jiao Liu, Tatia M C Lee, Jing Tao, Alex W K Wong, Bolton K H Chau, Lidian Chen, and Chetwyn C H Chan

NeuroImage 226 (2021) 117556

Contents lists available at ScienceDirect

NeuroImage

journal homepage: www.elsevier.com/locate/neuroimage

Fronto-cerebellar connectivity mediating cognitive processing speed ☆

Clive H.Y. Wong [a,b,c,1], Jiao Liu [d,e,f,l,1], Tatia M.C. Lee [b,c,j,k], Jing Tao [d,e,l], Alex W.K. Wong [g,h], Bolton K.H. Chau [a,i], Lidian Chen [d,e,l,*], Chetwyn C.H. Chan [a,i,*]

[a] Applied Cognitive Neuroscience Laboratory, Department of Rehabilitation Sciences, The Hong Kong Polytechnic University, Hong Kong
[b] Laboratory of Neuropsychology and Human Neuroscience, Department of Psychology, The University of Hong Kong, Hong Kong
[c] The State Key Laboratory of Brain and Cognitive Sciences, The University of Hong Kong, Hong Kong, China
[d] College of Rehabilitation Medicine, Fujian University of Traditional Chinese Medicine, 1 Huatuo Road, Minhou Shangjie, Fuzhou, Fujian 350122, China
[e] National-Local Joint Engineering Research Center of Rehabilitation Medicine Technology, Fujian University of Traditional Chinese Medicine, Fuzhou, China
[f] Department of Psychiatry, Massachusetts General Hospital and Harvard Medical School, Boston, United States
[g] Program in Occupational Therapy, Washington University School of Medicine, St. Louis, United States
[h] Department of Neurology, Washington University School of Medicine, St. Louis, United States
[i] University Research Facility in Behavioral and Systems Neuroscience, The Hong Kong Polytechnic University, Hong Kong
[j] The Affiliated Brain Hospital of Guangzhou Medical University, Guangzhou, China
[k] Center for Brain Science and Brain-Inspired Intelligence, Guangdong–Hong Kong–Macao Greater Bay Area, Guangzhou, China
[l] Key Laboratory of Orthopedics & Traumatology of Traditional Chinese Medicine and Rehabilitation (Fujian University of Traditional Chinese Medicine), Ministry of Education

ARTICLE INFO

Keywords:
Processing speed
Individual differences
Connectivity
Medial frontal cortex
Cerebellum

ABSTRACT

Processing speed is an important construct in understanding cognition. This study was aimed to control task specificity for understanding the neural mechanisms underlying cognitive processing speed. Forty young adult subjects performed attention tasks of two modalities (auditory and visual) and two levels of task rules (compatible and incompatible). Block-design fMRI captured BOLD signals during the tasks. Thirteen regions of interest were defined with reference to publicly available activation maps for processing speed tasks. Cognitive speed was derived from task reaction times, which yielded six sets of connectivity measures. Mixed-effect LASSO regression revealed six significant paths suggestive of a cerebello-frontal network predicting the cognitive speed. Among them, three are long range (two fronto-cerebellar, one cerebello-frontal), and three are short range (fronto-frontal, cerebello-cerebellar, and cerebello-thalamic). The long-range connections are likely to relate to cognitive control, and the short-range connections relate to rule-based stimulus-response processes. The revealed neural network suggests that automaticity, acting on the task rules and interplaying with effortful top–down attentional control, accounts for cognitive speed.

1. Introduction

Processing speed is a measure of cognitive ability and an index reflecting the severity of various neurological pathologies. Psychometric studies have revealed that common latent factors exist among all common speed measures (Roberts and Stankov, 1999), and processing speed (PS) mediates working memory and executive functions (Verhaeghen, 2011). Functional MRI studies (Forn et al., 2009; Habeck et al., 2016) have shown that processing speed tasks with different task demands activate frontal, parietal, and occipital cortices and the cerebellum, which is known as a task-positive network (Fox et al., 2005). In the current study, we investigated the interactions among the interregional brain activities within the TPN associated with the speed-related processes.

Using psychometric paradigms, such as digit–symbol substitution and symbol search tasks (Wechsler, 1981), faster processing speed was found to be commonly associated with decreased activations in the dorsal and medial frontal cortices but increased activations in the ventral lateral prefrontal cortex (PFC) and the insular, parietal and occipital regions (Akbar et al., 2016; Forn et al., 2013; Motes et al., 2011; Rypma et al., 2006; Sweet et al., 2005; Woodward et al., 2013). These studies further suggested that faster processing speed involves reduced

☆ Cognitive Processing Speed

E-mail addresses: hycwong@gmail.com (C.H.Y. Wong), liujiao0415@outlook.com (J. Liu), tmclee@hku.hk (T.M.C. Lee), taojing01@163.com (J. Tao), wongal@wusm.wustl.edu (A.W.K. Wong), bolton.chau@polyu.edu.hk (B.K.H. Chau), cld@fjtcm.edu.cn (L. Chen), Chetwyn.Chan@polyu.edu.hk (C.C.H. Chan).
[1] Co-first author and equal contribution
* Corresponding authors.

https://doi.org/10.1016/j.neuroimage.2020.117556
Received 30 July 2020; Received in revised form 2 November 2020; Accepted 6 November 2020
Available online 13 November 2020

reliance of executive function and efficient visuospatial processes. Findings of other studies using reaction time (RT) tasks, however, revealed negative speed-activation correlates were only found in the medial and dorsal frontal cortices (Hahn et al., 2007; Hu et al., 2014; Naito et al., 2000), which raises the question of the factors behind the inconsistent findings on the neural substrates that showed increases in activations, such as those in the occipital region. Paradigm- and stimulus-specific speed-RT correlates were previously reported, such as the lingual gyrus in a phonological go/no-go paradigm (Zhang et al., 2018) and the fusiform area in a visual letter search task (Madden et al., 2007) and the ventral lateral PFC in an audial choice RT task with syllables (Binder et al., 2004). Therefore, we conjecture that task-specific content, such as visual modality, and processing, such as search and comparison, are likely to contribute to the existing inconsistent findings of processing speed.

Functional connectivity (FC) is commonly used to identify interregional interactions, which are nondirectional and have zero-lag correlation. Independent component analysis on FC revealed that faster processing speed showed decreased coactivation of the frontoparietal component (Forn et al., 2013) and increased coactivation of the visual and cerebellar components (Silva et al., 2019). Two other common FC methods are Pearson's correlation (e.g. Gao et al., 2020) and psychophysiological interaction (e.g. Takeuchi and Kawashima, 2012). One prominent drawback of these methods, which are based on bivariate connectivity, is the possible over-representation of the interregional relationships (Sanchez-Romero and Cole, 2020) and intertwined activations among the identified neural substrates (Reid et al., 2019). Methods for tackling the issues mentioned can be applying effective connectivity (EC) and/or multivariate methods to the analyses, which are able to delineate concurrent and complex activations in multiple neural substrates, such as partial correlation (Smith et al., 2011) and vector autoregression (Deshpande et al., 2010). No study on processing speed has been found using a multivariate method. When compared with FC, EC is directional and has non-zero lag correlation, which can further characterize the task-related interregional coupling. Granger causality on EC showed higher processing efficiency was associated with decreased influences from dorsal PFC to posterior regions (Biswal et al., 2010; Rypma et al., 2006). Analyzing RT-correlates with FC revealed shorter RTs positively correlated with connectivity among the nodes of the dorsal attention networks (DAN, bilateral frontal eye-field and intraparietal sulcus, Corbetta and Shulman, 2002) and the ventral attention network (VAN, right anterior and posterior middle frontal gyrus, and right temporoparietal junction, Corbetta and Shulman, 2002). In the same study, the results of the EC revealed stronger DAN→VAN and weaker VAN→DAN influences that positively correlated with shorter RTs. Additional results brought by effective connectivity largely enrich the specificity and robustness of neural activities underlying processing speed.

The present study aimed to address the possible task-related biases by employing a series of simple stimulus–response (S–R) mapping tasks of visual and audial modalities. The purpose of this multitask design was to address the modality- and function-specific biases mentioned above. The arrow task (Lee et al., 2006; 2005), originally a visual S–R compatibility task, was adapted into visual and audial forms (Fig. 1). Responses involved simple reactions with respect to what was viewed or heard for better control of the required sensorimotor processing time (Jensen, 2006). A block, rather than event-related design, was employed to minimize the task-switching effect (Barber and Carter, 2004; Liu et al., 2015) and across-trial uncertainty (Bates and Stough, 1998; Fan, 2014). Furthermore, we aimed to address the methodological shortfalls in previous studies that utilized Pearson's correlation and psychophysiological interaction (PPI) for building connectivity-based models to predict processing speed. In this study, we established six connectivity measures, including four multivariate-based indices, for conducting the model comparisons. A cognitive speed variable was constructed by regressing out the RT of the control tasks from that of the experimental tasks for controlling the sensorimotor components. The functional connectivity model building was based on mixed-effect LASSO regression. To our knowledge, this paper is the first in the field to employ the cross-modality multitask design and to compare results yielded from six methods for modeling the interregional interactions' subserving processing speed.

2. Method

2.1. Participants

Forty healthy young adults aged 18–28 were recruited from local communities to participate in the study. They all had a high school education or higher. The final sample included 35 participants (21.5 ± 2.1 years, 14 females), with five participants excluded from the analysis. The reasons for the exclusion included missing or premature responses (< 100 ms) and error trials exceeding 30% of the trials in any one of the task conditions. All of the participants had normal or corrected-to-normal visual acuity based on the E Standard Logarithm Eyesight Table, as well as normal auditory ability determined by passing a pure-tone detection test at 300–1000 Hz octave frequencies. All participants were right-handed, based on the Edinburgh Handedness Questionnaire (Oldfield, 1971). They also passed screening tests for cognitive impairment (Montreal Cognitive Assessment, Beijing Version (Yu et al., 2012), MoCA < 26) and depressive mood (Hamilton Rating Scale for Depression (Frank et al., 1991), HAMD ≥ 7) and had no known history of neurological diseases, substance abuse, or smoking. No MRI scan contraindications were identified. Each participant was informed of the purposes of the study, and informed consent was obtained prior to the training and experimental procedures. Ethical approval was obtained from the Ethics Committee of Fujian University of Traditional Chinese Medicine.

2.2. Processing speed task

The Arrow Task (Lee et al., 2005; 2006) was used to measure the processing speed. It involved a two-choice S–R mapping task with compatible (COM), incompatible (INC), and simple RT control conditions (NEU) (Fig. 1). In the COM, the participant pressed the "UP" button when an upward arrow appeared and the "DOWN" button when a downward arrow appeared (Fig. 1). In the INC, the participant pressed the "UP" button for a downward arrow and the "DOWN" button for an upward arrow. The NEU involved the participant pressing any button upon viewing a vertical line without an arrowhead. As the stimuli that appeared in these conditions were visual images, they were called COM-VIS, INC-VIS, and NEU-VIS. The audial version of the same conditions were COM-AUD, INC-AUD, and NEU-AUD, with upward arrows, downward arrows, and vertical lines replaced with high-pitch, low-pitch, and mid-pitch tones, respectively. The task trials were organized using a block design, with five blocks in each of the three visual and audial conditions. The visual run had 15 visual blocks, and the audial run had 15 audial blocks. The three task blocks were arranged in an A-B-C-A-B-C sequence, and the task conditions were counterbalanced across the participants. Each block included 10 trials, with an equal number of trials for the COM and INC mapping rules, presented in randomized order. There were 50 trials in each of the 3 × 2 task conditions. Instructions for the conditions were presented to each participant for 4 s preceding each block. For each trial, the stimulus was presented for 800 ms, followed by a fixation of 1000 ms, during which time the response was made. Each block was completed in 18 s. The total duration for completing one run was 350 s. The resting period between each run was 10 s.

2.3. Analysis of behavioral data

Trials with RTs shorter than 100 ms were excluded from the analyses. Mean RTs were calculated by fitting the RTs of the correct trials. Accuracy rate (ACC) was defined as the number of accurate trials divided by the number of accepted trials. The RT and ACC data were fit-

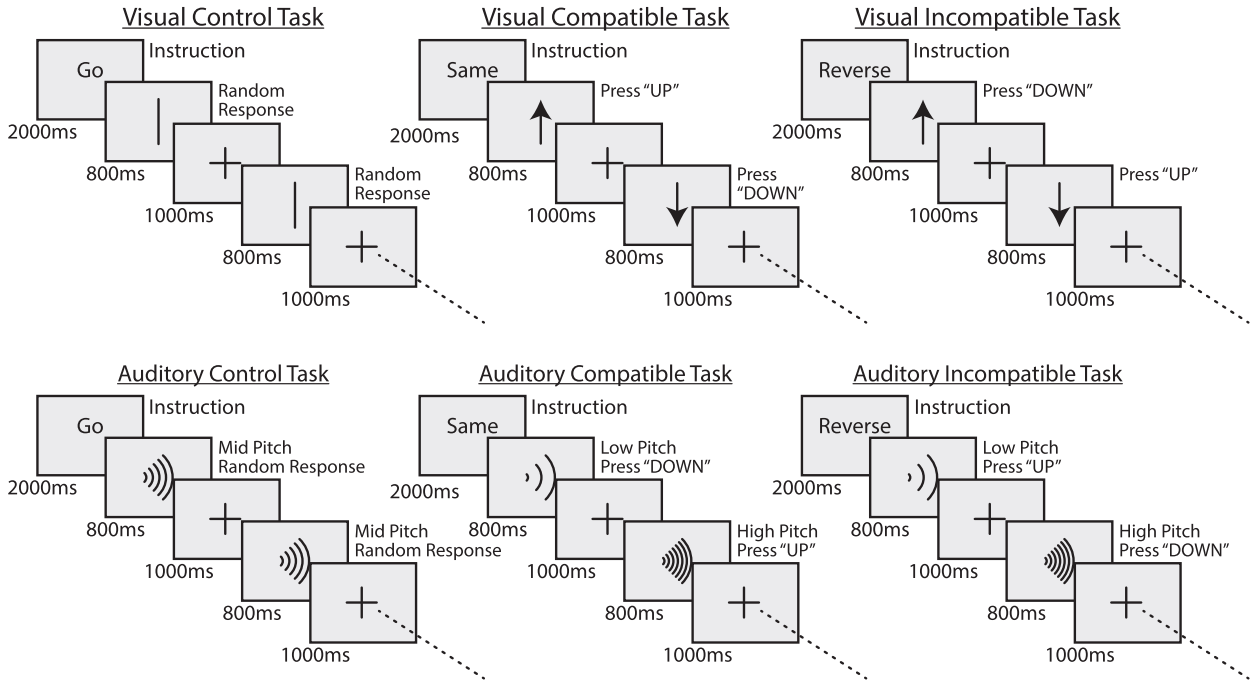

Fig. 1. Schematic diagram describing the adapted Arrow Task in three conditions (compatible, incompatible, and control) crossed with two modalities (visual and audial).

ted to a linear mixed model, where subjects were modelled as a random effect. The model was fitted with the "lme4" R package. Post hoc pairwise comparisons were conducted on all significant effects and corrected with Tukey's test implemented in the "emmeans" R package.

2.4. Definition of processing speed and cognitive speed

Conventionally, PS is measured as the duration between the onset time of the stimulus and the behavioral response. However, sensory and motor time should be accounted to tap into higher cognitive demand (Jensen, 2006). Cognitive speed (CS) is defined by regressing out the simple RT of the corresponding perceptual modality from the RT measured by the Arrow Task (Jensen and Reed, 1990). The RTs for each of the four experimental conditions (compatible/incompatible × visual/audial) and the RTs for each of the control conditions (visual/audial) were fitted into the linear mixed model:

$$\boldsymbol{y} = \boldsymbol{X\beta} + \boldsymbol{Zb} + \varepsilon$$

where y is a vector of the task RT, X is a matrix of the RTs of the two control conditions, Z is a matrix of the RTs of the four experimental conditions, and the ε is extracted from the model as the corrected RTs (i.e., CSs). Previous studies employed a similar procedure for extracting PS from paper-and-pen tests (Kansal et al., 2017) and computerized tasks (Roth et al., 2015). The formula above yielded two speed indices, in which higher values reflected faster speeds. The ex-Gaussian model was fitted with the "retime" R package, and the model was fitted with the "lme4" R package.

2.5. MRI scanning parameters and data preprocessing

MRI images were acquired from a GE Signa HDxt 3T scanner (General Electric, Milwaukee, WI, USA) with an eight-channel phased-array head coil. A high-resolution anatomical image (MP-RAGE, field of view = 240 × 240 mm, slice thickness = 1 mm, gap = 0 mm, slices = 160 axial slices, acquisition matrix = 256 × 256, TR/TE = 5556/1764 ms, inversion time = 450 ms, and flip angle = 15°) and two functional EPI runs (axial acquisition, field of view = 240 × 240 mm, slice thickness = 4 mm, gap = 0 mm, slices = 40 axial slices, acquisition matrix = 64 × 64, TR/TE 2000/30 ms, number of volumes = 175, and flip angle = 90°) were acquired for each subject.

The session-level analysis was completed with FSL/FEAT (version 5.0.9) (Jenkinson et al., 2012). Scanner instability and drifting were reduced by removing the beginning five volumes and applying a high-pass filter of 1/90 Hz for each run. Head movement artifacts were reduced by aligning each volume to the middle volume. Spatial noises were reduced by applying a 5-mm FWHM Gaussian. Artifactual components were removed through visual inspection (Kelly et al., 2010) of the independent components obtained with MELODIC. BOLD signals were fitted with gamma-convoluted task models and nuisance regressors, including head motion and temporal derivatives. Two task-to-baseline contrasts were obtained. The ICA-cleaned functional imaging data is available at https://github.com/clivehywong/2021CPS.

Spatial normalizations were performed using Advanced Normalization Tools version 2.2.0 (Avants et al., 2014) with the MNI template. Field inhomogeneity in the mean functional and structural images of each subject were corrected with N4BiasFieldCorrection. The functional-to-structural rigid transformation matrix and structural-to-template high-dimensional diffeomorphic deformation were calculated with antsIntermodalityIntrasubject.sh and antsRegistrationSyN.sh (transformation matrix and deformation field are available at https://github.com/clivehywong/2021CPS). The latter implemented the symmetric normalization method (Avants et al., 2008), which is regarded as having the best performance among similar tools (Klein et al., 2009). All contrasts of parameter estimates (COPEs) predicted from FEAT were normalized to the MNI template, combining rigid and diffeomorphic transformations by antsApplyTransforms for the extraction of activations of the regions of interest (ROIs).

2.6. Defining regions of interest

The ROIs submitted for analyses in this study were based on the activation maps generated from three PS tasks (Razlighi et al., 2017) and were retrieved from NeuroVault (https://identifiers.org/neurovault.collection:857). These PS tasks

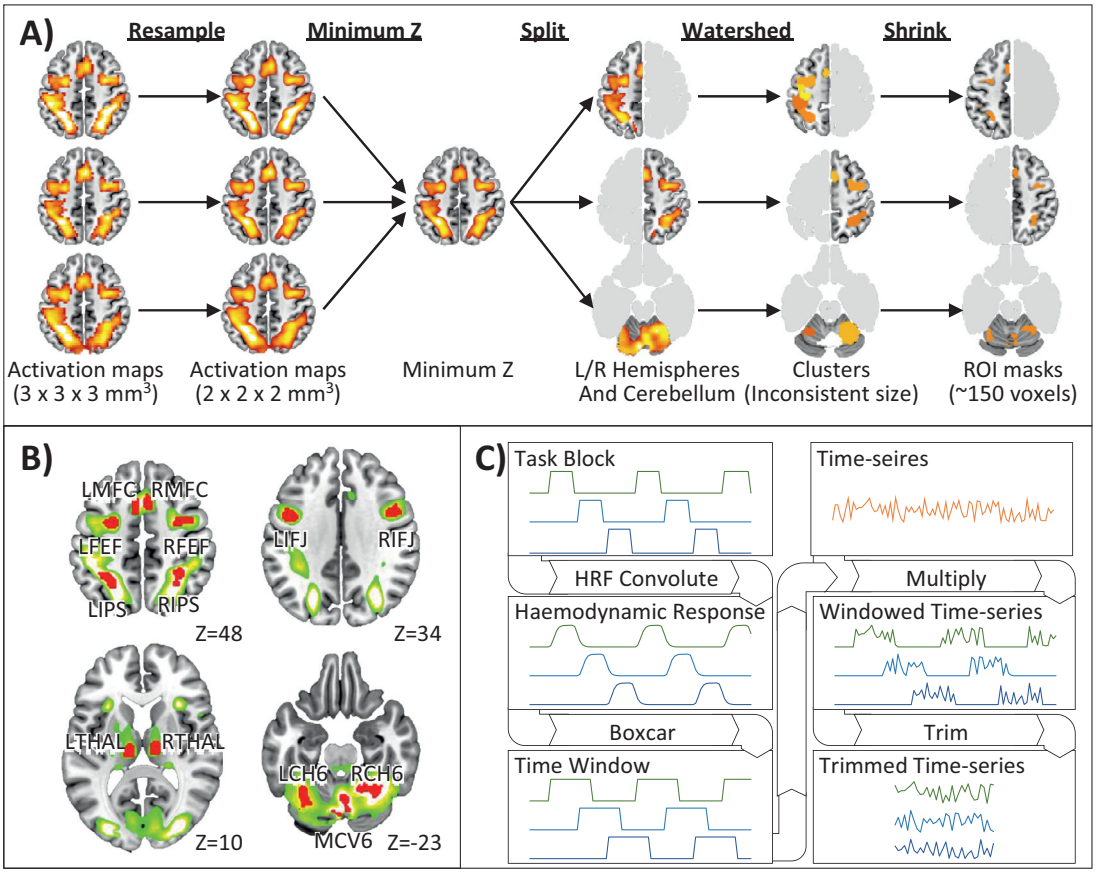

Fig. 2. Schematic diagram for regions of interest and time-series data extraction. (A) The workflow for extracting the ROIs. (B) Selected ROI masks based on the activation maps of digit–symbol, letter comparison, and pattern comparison tasks reported by Razlighi et al. (2017); the green–yellow gradient represents minimum Z values; the red cluster represents ROI masks. (C) Extraction of task-specific time-series data. LMFC: left medial frontal cortex. RMFC: right medial frontal cortex. LFEF: left frontal eye field. RFEF: right frontal eye field. LIFJ: left inferior frontal junction. RIFJ: right inferior frontal junction. LIPS: left intraparietal sulcus. RIPS: right intraparietal sulcus. LTHAL: left thalamus. RTHAL: right thalamus. LCH6: left cerebellar hemisphere lobule VI. RCH6: right cerebellar hemisphere lobule VI. MCV6: medial cerebellar vermis VI.

were digit–symbol, letter comparison, and pattern comparison. The detailed task-taking processes of each task can be found in the work of Razlighi et al. (2017). In brief, the digit–symbol task involved pairing digits to symbols, and the letter and pattern comparison tasks involved matching two strings or figures, respectively. Participants responded by pressing designated buttons on a response pad.

The activation maps were resampled to 2 mm isotropic voxels, and the voxel-wise minimum Z was calculated. Each map was split into left/right hemispheres and cerebellum to ensure anatomical homogeneity of the ROI masks. The maps were then parsed into smaller regions using the watershed method (Satterthwaite et al., 2013). The initial Z threshold and the merging threshold were set to 10 and 13, respectively, and the dropping and merging thresholds were set to 100. This enabled clusters with smaller than 100 voxels to be merged with the neighboring clusters or removed. To mitigate the inhomogeneity introduced by the inconsistent and extended sizes of the ROIs, the clusters were shrunk to approximately 150 voxels by increasing the Z threshold from 11 to 18 with a step of 0.05 by using an in-house script (Arslan et al., 2018). The cluster forming procedure is illustrated in Fig. 2A, and the extracted ROIs are shown in Fig. 2B.

2.7. Activation and connectivity predictors

Six sets of interregional connectivity measures and the regional activation were estimated. Activation predictors were extracted from the parameter estimates of the first-level contrasts. Generalized psychophysiological interaction (gPPI) was estimated with the original time series, and the rest of the measures were calculated with windowed time series. Pearson's correlations were estimated with the "base" R package; partial and semi-partial correlations were estimated with the "ppcor" R package. For directed path predictors, including gPPI, semi-partial correlations, and first- and second-order multivariate vector autoregression (VAR(1) and VAR(2)), after solving the equations for the n ROIs, a $n \times n$ matrix with dimension n^2 was obtained. The coefficients representing self-loops were excluded from the analysis, leaving $n^2 - n$ path coefficients. For undirected path predictors, the lower triangle was a mirror of the upper triangle of the $n \times n$ matrix, and only the upper triangle was retained, leaving $n \times (n-1)/2$ path coefficients. The code for the connectivity estimation is available at https://github.com/clivehywong/2021CPS.

2.8. Extraction of task-specific windowed time series

Task-specific windowed time series were required for the correlation-based and vector autoregression-based connectivity estimations. BOLD signals within each ROI mask were extracted by averaging the signal for all voxels inside the mask (Fig. 2B). The initial boxcar function of the task blocks was convoluted with the hemodynamic response function, and the convoluted series were then converted into square waves with a boxcar function. The time series were multiplied to the square waves of each individual task to obtain

a windowed time series. The windows were concatenated to form the final task-specific time series (Fig. 2C).

2.9. Connectivity modelled with generalized psychophysiological interaction

The gPPI analysis was adapted to estimate contextual functional connectivity using a linear model:

$$x_j(t) = a_{ij} + b_{ij}y_k(t) + c_i x_i(t) + d_i y_k(t)x_i(t) + \varepsilon_i(t)$$

where $x_i(t)$ and $x_j(t)$ are the mean-centered time series of ROI_i (the physiological term) and ROI_j; $y_k(t)$ is the HRF task regressor for task k (the psychological term); a_i is the intercept; b_i, c_i, and d_i are the parameter estimates for the psychological, physiological terms, and interaction term; and $\varepsilon_i(t)$ is the error term. The parameter estimate d_i was extracted as the connectivity measure from ROI_i to ROI_j. Parameters were estimated with lm in the "stat" R package.

2.10. Connectivity modelling with vector autoregression

For a network of n ROIs, the p-th order vector autoregressive model VAR(p) is modelled:

$$x_i(t) = c_i + \sum_{j=1}^{n}\sum_{k=1}^{p}\alpha_{ijk}x_i(t-k) + \varepsilon_i(t)$$

where the endogenous variable $x_i(t)$ is the time series of region i; c_i is the intercept of $x_i(t)$; α_{ijk} is the effect of region j on region i with a lag of k time points; and $\varepsilon_i(t)$ is the residual time series at region i. Hence, the first-order vector autoregressive model VAR(1) is modelled as follows:

$$x_i(t) = c_i + \sum_{j=1}^{n}\alpha_{ij1}x_i(t-1) + \varepsilon_i(t)$$

The second-order model VAR(2) is modelled as follows:

$$x_i(t) = c_i + \sum_{j=1}^{n}\alpha_{ij1}x_i(t-1) + \sum_{j=1}^{n}\alpha_{ij2}x_i(t-2) + \varepsilon_i(t)$$

The solution involved one $n \times n$ matrix for each lag. Only the matrix containing α_{ij2} was retained for the VAR(2). The VAR path coefficients were estimated with the "vars" R package, and the implementation was adapted from "1dGC" of the AFNI package. The stationarities of 70 (35 participants x 2 sessions) time series were confirmed with KPSS and ADF with the "tseries" R package, and the degree of lagging was estimated with Akaike criteria (AIC; (Pfaff, 2008), with maximum lagging of 5 for the 140 models. The results suggested that VAR(1) and VAR(2) were both plausible orders for vector autoregression (Table S1). The order of lagging corresponded to the TR of the fMRI acquisition. Hence, VAR(1) represented a lag of 2 s, and VAR(2) represented a lag of 4 s.

2.11. Linear mixed-model lasso for variable selection

We established 12 models by predicting the speed indices PS and CS from each of the six sets of connectivity measures: Pearson's, partial, semi-partial correlations, PPI, VAR(1), and VAR(2). Firstly, for each of the connectivity matrices, connectivity paths that survived one-sample t-test with $p \leq 0.05$ were included in the model testing. The number of predictors for the model, denoted as p, was less than or equal to 78 and 156 for the non-directed and directed connectivity measures, respectively (pairwise combinations of 13 ROIs depending on the statistical significance of paths ≤ 0.050). A significant speed-connectivity correlation was defined as all subjects showing consistent positive connectivity for the same path (Fig. 3C). Secondly, linear mixed-model LASSO regression was applied for variable selection using the "glmmLasso" R package. In each model, the dependent variables were the 140 speed indices (35 subject x 4 conditions), and the fixed-effect independent variables were the estimated connectivity indices of each path for each condition. These formed a matrix with [p x 140] dimensions. The task conditions were modelled as random intercepts. Before the model selection procedure, all variables were first converted to standard score. The tuning parameter λ was iterated from 100 to 1 with a step of −1 (Groll and Tutz, 2014). The initial λ of each model was ascertained to suppress the coefficients to zero. In each iteration, the delta and q parameters from the previous iteration were used to initialize the LASSO fitting. The parameter λ of the final solution was chosen according to AIC criteria to estimate the Fisher scoring. Variables with non-zero coefficients were then fitted to a linear mixed-effects model using the "lme4" R package. Confidence intervals were estimated with 5000 bootstraps, and the effect sizes were calculated using Cohen's f^2 (Selya et al., 2012).

Table 1
Mean reaction times and accuracy rates for the Arrow Tasks.

		Auditory		Visual	
	Task	Mean	SD	Mean	SD
Reaction Times (ms)	NEU	240	83	245	45
	COM	366	84	380	46
	INC	403	97	443	61
Accuracy Rates (%)	NEU	100	0	100	0
	COM	96.0	6.4	96.9	4.6
	INC	96.2	3.7	96.8	2.8

NEU: control condition. COM: compatible condition. INC: incompatible condition.

2.12. Predictive models and model comparison

In the current study, the six sets of activation and connectivity predictors were used to predict each of the two speed indices. Twelve models were estimated, and the performance of the models were compared using the AIC obtained from an ANOVA test against the corresponding null model. Goodness of fits of the mixed-effects models were estimated with the marginal R-square value from the "MuMIn" R package. The marginal R-square represents only the variance explained by fixed factors (Nakagawa and Schielzeth, 2012). The code for the data analysis is available at https://github.com/clivehywong/2021CPS.

3. Results

3.1. Reaction times and accuracies

The Condition effect on the mean RTs was significant, $F(2, 170) = 353$, $p < 0.001$, while the Modality effect, $F(1, 170) = 2.4$, $p = 0.117$, and their interactions, $F(2, 170) = 1.4$, $p = 0.241$, were not significant (Table 1). Post-hoc analysis on Condition showed that the RT for NEU was significantly shorter than those of COM, $t(170) = 6.5$, $p < 0.001$, and INC, $t(170) = 19.0$, $p < 0.001$, and the RT of COM was significantly shorter than that of INC, $t(170) = 25.6$, $p < 0.001$. For accuracy rate, the Condition effect, $F(2, 170) = 24.7$, $p > 0.001$, was significant, but the Modality effect, $F(1, 170) = 1.1$, $p = 2.8$, and their interactions, $F(2, 170) = 0.3$, $p = 0.730$, were not significant. Post hoc analyses on Condition showed that the accuracy for NEU was significantly higher than those of COM, $t(170) = 6.1$, $p < 0.001$, and INC, $t(170) = 6.0$, $p < 0.001$, and the difference between the accuracies of COM and INC was not significant, $t(170) = 0.055$, $p = 0.998$.

3.2. Regions of interest

Thirteen ROIs were selected (Fig. 2B, Table 2, available at https://github.com/clivehywong/2021CPS), including frontal (bilateral medial frontal cortex, bilateral frontal eye field, and bilateral inferior frontal junction), parietal (bilateral intraparietal sulcus), subcortical (bilateral thalamus), and cerebellum (bilateral lobule 6 and vermis 6). The number of voxels ranged from 148 to 155.

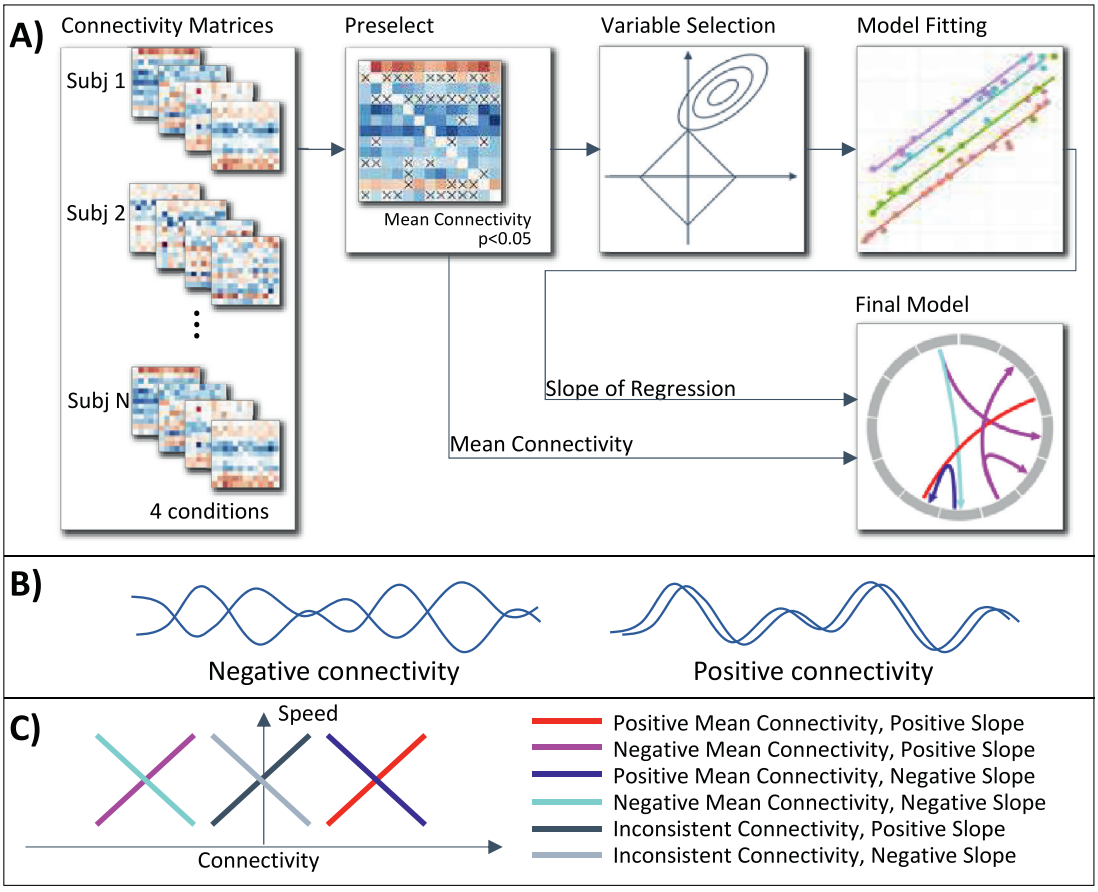

Fig. 3. Model estimation procedure. A) Estimated connectivity matrices for each condition for each subject. Each element in the matrices is subjected to a one-sample *t*-test, and statistically significant paths are selected ($p < 0.05$). LASSO regressions are conducted for feature selection, and selected paths are then fitted to a linear mixed model. Direction of connectivity and slope of speed-connectivity regression are combined. B) Illustration of negative and positive connectivity. C) Illustration of regression lines that combine direction of connectivity with slope of speed-connectivity correlates. Light and dark gray lines represent connectivities that have inconsistent positive or negative connectivity and are therefore excluded from the significant model.

Table 2
Details of the region of interests.

Label	Substrate	vox	Vol	MNI coordinate (X, Y, Z)		
LMFC	Left Medial Frontal Cortex	155	1240	−5.8	8.3	51.1
LFEF	Left Frontal Eye-Field	150	1200	−28.8	−4.4	51.2
LIFJ	Left Inferior Frontal Junction	153	1224	−44.8	2.7	34.2
LIPS	Left Intraparietal Sulcus	155	1240	−30.8	−50.5	45.0
LTHAL	Left Thalamus	153	1224	−11.6	−19.6	9.2
LCH6	Left Cerebellum Lobule 6	154	1232	−30.5	−59.7	−25.5
MCV6	Cerebellum Vermis 6	153	1224	2.0	−68.6	−20.1
RCH6	Right Cerebellum Lobule 6	150	1200	24.5	−53.0	−22.1
RTHAL	Right Thalamus	153	1224	11.9	−17.1	10.5
RIPS	Right Intraparietal Sulcus	154	1232	31.5	−49.5	45.0
RIFJ	Right Inferior Frontal Junction	150	1200	45.0	6.7	32.7
RFEF	Right Frontal Eye-Field	148	1184	35.4	−2.5	50.3
RMFC	Right Medial Frontal Cortex	155	1240	5.2	13.1	49.4

Note: vox: number of voxel in the cluster. Vol: volume of the cluster, in mm^3.

3.3. Model comparison

The accuracy metrics of the best models selected by LASSO for each set of connectivity predictors are listed in Table 3. All models are significantly better than the corresponding null models, as indicated by the AIC of the ANOVA tests. The model built with VAR(1) attained the lowest AIC for PS (AIC = 368.0, R^2 = 0.212) and CS (AIC = 365.1, R^2 = 0.374). Because the AIC for different dependent variables are not directly comparable, we cannot compare the best models of PS and CS with it. The marginal R^2 values indicated that the CS ~ VAR(1) model attained the highest explained variance among all the models.

3.4. Selected model: predicting cognitive speed with first-order vector autoregression

The selected model predicted CS from interregional interaction modelled with first-order vector autoregression: $\chi^2(21) = 73.2$, $p < 0.001$, and R^2 = 0.374. The final model involved 21 predictors, six of which were significant (Table 4 and Fig. 3). The paths that predicted faster

Table 3
Comparison of accuracy metrics of LASSO-selected models built with different fMRI-derived activation/connectivity variables.

					Chi-Square Test			
Connectivity measure	Abbv	Df	AIC	R^2	χ^2	Df	p	-log(p)
Processing Speed								
Null Model		3	392.6					
BOLD	PS~BOLD	7	377.9	0.137	22.6	4	0.00015	3.83***
gPPI	PS~gPPI	8	373.7	0.160	28.8	5	2.51E-05	4.6***
Pearson Correlation	PS~Pearson	18	376.1	0.225	46.5	15	4.46E-05	4.35***
Partial Correlation	PS~Partial	11	375.4	0.183	33.1	8	5.80E-05	4.24***
Semi-partial Correlation	PS~Semi-Partial	10	374.4	0.176	32.1	7	3.86E-05	4.41***
VAR(1)	PS~VAR(1)	11	**368.0**	0.212	40.5	8	2.54E-06	5.60***
VAR(2)	PS~VAR(2)	9	384.3	0.114	20.3	6	0.00245	2.61**
Cognitive Speed								
Null Model		3	402.3					
BOLD	CS~BOLD	7	397.0	0.088	13.3	4	0.00977	2.01**
gPPI	CS~gPPI	12	386.3	0.205	34.0	9	8.89E-05	4.05***
Pearson Correlation	CS~Pearson	12	394.8	0.157	25.5	9	0.00248	2.61**
Partial Correlation	CS~Partial	8	386.3	0.165	26.0	5	8.88E-05	4.05***
Semi-partial Correlation	CS~Semi-Partial	8	383.8	0.179	28.5	5	2.91E-05	4.54***
VAR(1)	CS~VAR(1)	21	**365.1**	**0.374**	73.2	18	1.31E-08	7.88***
VAR(2)	CS~VAR(2)	4	395.9	0.058	8.4	1	0.00369	2.43**

Note: The models were abbreviated with the notation *dependent variable ~ independent variable set*. PS: Processing speed index. CS: Cognitive speed index. BOLD: brain activations. gPPI: generalized psychophysiological interaction network estimates. Pearson: Pearson correlation network estimates.

Table 4
LASSO-selected variables of the model predicting speed with effective connectivities estimated with first-order vector autoregressions.

Predictors	Cohen's f^2	Conn	β	SE	95% CI	p
RMFC→LIPS	0.232	−0.049	0.301	0.110	[0.086, 0.517]	0.007**
RMFC→MCV6	0.222	−0.047	−0.330	0.125	[−0.585, −0.080]	0.010**
LIFJ→RCH6	0.202	0.051	0.218	0.091	[0.043, 0.395]	0.017*
MCV6→RCH6	0.196	0.169	−0.193	0.082	[−0.362, −0.030]	0.021*
LCH6→LTHAL	0.182	−0.094	0.226	0.104	[0.019, 0.432]	0.031*
LCH6→LFEF	0.176	−0.148	0.241	0.114	[0.016, 0.461]	0.036*

Note: Only significant paths are shown in the table. Conn: the mean of the connectivity estimates, positive value represents positive interregional interaction and vice versa; β: the parameter estimates of the regression model; se: standard error; 95%CI: 95% confidence interval. Also see Fig. 4.

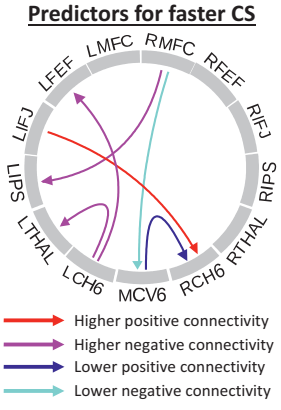

Fig. 4. The connectivity predictors of the best models for CS using VAR(1) predictors. Only significant connections are plotted on the figure.

CS were higher negative RMFC→LIPS (Cohen's f^2 = 0.232, Mean Connectivity = −0.049, β = 0.301, 95% CI: [0.086, 0.517], and p = 0.07), lower negative RMFC→MCV6 (Cohen's f^2 = 0.222, Mean Connectivity = −0.047, β = −0.33, and p = 0.01), higher positive LIFJ→RCH6 (Cohen's f^2 = 0.202, Mean Connectivity = 0.051, β = 0.218, 95% CI: [0.043, 0.395], and p = 0.017), lower positive MCV6→RCH6 (Cohen's f^2 = 0.196, Mean Connectivity = 0.169, β = −0.193, 95% CI: [−0.362, −0.03], and p = 0.021), higher negative LCH6→LTHAL (Cohen's f^2 = 0.182, Mean Connectivity = −0.094, β = 0.226, 95% CI: [0.019, 0.432], and p = 0.031), and higher negative LCH6→LFEF (Cohen's f^2 = 0.176, Mean Connectivity = −0.148, β = 0.241, 95% CI: [0.016, 0.461], and p = 0.036). Among the six interregional connectivity paths, three originated from the frontal region and three from the cerebellum.

4. Discussion

In this study, interregional interactions associated with PS were evaluated by predicting cognitive processing speed with two sets of speed indices and six sets of connectivity indices. The results indicated that the first-order vector autoregression model VAR(1) was a better model than the Pearson's, partial semi-partial correlations, psychophysiological interaction, or second-order VAR models. The most significant finding was, among the predefined task-positive network involving frontal, parietal and subcortical regions, a predominant cerebello-frontal network found to be associated with cognitive processing speed. The neural network was composed of six speed-related effective paths. Among them, three long-range functional connectivities between the frontal cortex and cerebellum were LIFJ→RCH6, RMFC→MCV6, and LCH6→LFEF. There were also three short-range connectivities, with two involving the cerebellum (i.e., MCV6→RCH6 and LCH6→LTHAL) and one involv-

ing the cortex (i.e., RMFC→LIPS). It is noteworthy that stronger predictions of the speed come from the frontal- rather than the cerebellar-originated connectivities. Higher positive connectivity of the LIFJ with the RCH6, lower negative connectivity of the RMFC with the MCV6, and higher negative connectivity of the RMFC with the LIPS resulted in faster speeds. These were compared with higher negative connectivity of the LCH6 with the LTHAL and LFEF and with lower positive connectivity of the MCV6 with the RCH6, which resulted in faster speed. The results suggest CS may involve interactions between effortful and automatic information processing subserved by the RMFC and LFEF (frontal drivers) and the LCH6 and RCH6 (cerebellar drivers), respectively.

4.1. Cognitive speed definition

This study was targeted at reducing the influence due to task specificity and isolating the portion of the time accounting for the speed of the cognitive processes. The "two-modality by three-task rule" would have reduced the task specificity; and the cognitive speed index derived would have partialled out the RTs of the control conditions from those of the experimental conditions (Kansal et al., 2017). The results demonstrate that the VAR(1) model was more useful for predicting the CS than for predicting the PS (see Table 3).

4.2. Connectivity networks

The yielded significant ROIs were found to overlap with the neural substrates commonly associated with the DAN (Corbetta and Shulman, 2002; i.e., RFEF, LFEF, LIFJ, RIFJ, LIPS, RIPS, LTHAL, and RTHAL) and CON (Cinguloopercular Network, Dosenbach et al., 2006; i.e., RMFC, LMFC, RCH6, MCV6, and LCH6). The connectivities revealed among the predefined task-positive ROIs suggest a plausible cerebello-frontal network within a predefined set of regions association with the CS. Interpretations of the effective connectivities revealed in this paper are based on two dimensions—uni- versus bidirectional—and the relationships of functional and anatomical connections reported in previous studies. For directions of causative connectivity, due to the complexity involved in reciprocal causation, this study only included task-positive nodes. This eliminated connectivity pairs that might have manifested as reciprocal causation in nature, keeping those that would have been unidirectional in nature. The lack of possible reciprocal or circular connectivities is a limitation of this study. The plausible neural processes underlying the identified effective connectivities is elaborated below.

The strongest effective connectivity predictors were the RMFC→LIPS, RMFC→MCV6, and LIFJ→RCH6. The latter two functional pairs were long-range, from frontal cortex to cerebellum. The other two functional pairs were short-range, which cluster in the cerebellum (i.e., MCV6→RCH6 and LCH6→LTHAL). The functional association of the cerebello-frontal network with CS is a new finding. Previous studies reported that effective connectivities of the cerebello-frontal network were related to a wide range of cognitive processing, such as visual (Kellermann et al., 2012) and auditory (Salmi et al., 2009) attention, perceptual timing prediction (O'Reilly, Mesulam, and Nobre, 2008), working memory (Luis et al., 2015), and executive function (Reineberg and Banich, 2016). Specific to PS, Eckert et al. (2010) reported structural speed–brain correlates in the cerebellar and frontal regions. Using source-based morphology on structural imaging data, seven structural components in the cerebellum and the frontal cortex associated with age-related changes in PS were identified. The findings of this study are consistent with those revealed by Eckert et al. (2010) and offer further evidence suggesting plausible cerebellar-frontal functional interactions for mediating PS.

The results suggest that the RMFC plays a significant role in facilitating CS, as it was part of two connectivity pairs: RMFC→MCV6 and RMFC→LIPS. In the RMFC→MCV6, lower negative connectivity of the RMFC with the MCV6 (or cerebellum vermis VI) predicted faster CS. This finding is somewhat consistent with previous studies, in which PS was associated separately with activations in the MFC (Forn et al., 2013) and vermis (Ruet et al., 2014; Silva et al., 2019) and with the cerebellar and frontal regions (Eckert, 2011; Paul et al., 2009). Nevertheless, the concurrent involvements of MFC and various cerebellar regions have also been reported in other intrinsic connectivity (Buckner et al., 2011; Habas et al., 2009), task connectivity (Forn et al., 2013), and meta-analytic (Bernard and Seidler, 2013) studies. Functionally, the RMFC was associated with proactive control (Clark et al., 2020; Hu et al., 2016) and inhibited competing task sets (Mayr et al., 2006), whereas the MCV6 was associated with vigilance attention (Langner and Eickhoff, 2013) and working memory speed (H. Ding et al., 2012). Excitatory stimulation of the medial cerebellum was found to increase attention performance (Esterman et al., 2017), and inhibitory stimulation hampered the automaticity of cognitive processes (Argyropoulos et al., 2011). The MFC (Korb et al., 2017; la Vega, Chang, Banich, Wager, and Yarkoni, 2016) and the posterior cerebellum (D'Mello et al., 2020) were found to associate with action- and motor-oriented cognitive control (Langner and Eickhoff, 2013). Taken together, the lower negative influence from the RMFC to the MCV6 (i.e. RMFC→MCV6) for faster CS may be due to the lowering of regulation from the frontal region, which could have facilitated the automaticity attention processes subserved by the cerebellum (Ramnani, 2014; Shine and Shine, 2014). In this study, higher negative influence from the RMFC to the LIPS (i.e. RMFC→LIPS) also predicted faster CS. This result is contrary to that of another study that reported faster PS associated with higher coactivation between the two regions (Forn et al., 2013). Effective MFC to LIPS connectivity was found to modulate cognitive control (Harding et al., 2015), while LIPS alone was involved in higher order goal-related action control (Tunik et al., 2007). The higher negative connectivity of RMFC with LIPS suggests that a faster CS would have involved increased suppression of irrelevant action-rule representations, such as the compatible rules ("UP" button when an upward arrow appeared) when performing the incompatible conditions in this study.

The involvement of the LCH6 and RCH6 in CS is an interesting and important finding. The LCH6 was found to form higher negative connectivities with the LFEF and LTHAL, which contributed to faster CS. The results are consistent with those reported in one study that activations of the LCH6 and LTHAL were associated with PS (Genova et al., 2009). Cerebellar-thalamic connectivity was associated with visuomotor control (Lin et al., 2009) and formation of motor memory (Mawase et al., 2017). The LCH6 was frequently associated with spatial processing, working memory, and low cognitive demand tasks with overt movements (Stoodley et al., 2012). A recent review on the functions of thalamus suggest its role is beyond the relay of cortico-cortical information (Guillery and Sherman, 2002) but participates in sensorimotor integration (Murray et al., 2012). Previous studies on PS also reported thalamus involvement among older adults (Waiter et al., 2008) and patients with multiple sclerosis (Bisecco et al., 2017). The association between the higher negative connectivity of the LCH6 with the LTHAL (i.e. LCH6→LTHAL) suggests that a faster speed might have required inhibition of the thalamus for participating in the task-taking processes (Prevosto and Sommer, 2013). This proposition is inconsistent with the task employed in this study, requiring a low level of attention and simple task sets for producing overt motor responses. The FEF has been functionally associated with top–down reorientation of attention (Shulman et al., 2009) and encoding of multimodal stimuli (Spagna et al., 2015; Tamber-Rosenau et al., 2013), such as visual and auditory stimuli (Tark and Curtis, 2009). The higher negative connectivity findings of the LCH6 with LTHAL and LFEF suggest that faster CS might have involved inhibition of the frontal cortical activities for keeping pace with the cognitive demands, as required by the multimodal attentional task of this study. Our findings contextualize the possible inhibitory role played by the cerebellum on the frontal and subcortical neural substrates for fostering faster CS.

Different from the LCH6, the RCH6 was the recipient of positive connectivity from the LIFJ and MCV6. It suggests that involvements

of RCH6 may be facilitated, rather than inhibited, by the activations of the frontal cortex and cerebellum. A recent meta-analytic study reported that the LIFJ was associated with reactive control (Clark et al., 2020), while the RCH6 was associated with working memory speed (Salmi et al., 2010). The IFJ and RCH6 were related to maintaining (Woolgar et al., 2011) and implementing (Balsters and Ramnani, 2011) stimulus–response task rules. The higher positive connectivity of the LIFJ with the RCH6 (i.e. LIFJ→RCH6) suggests that frontal activations would have facilitated faster task-rule responses subserved by the RCH6. The results of the present study do not support three proposed cerebellar connectivities: LIFJ→RCH6, RCH6→LFEF, and LCH6→LTHAL. Plausible reciprocal cortico-cerebello-cortical connectivity of the LIFJ→RCH6 and RCH6→LFEF influencing CS warrants future investigation. The significant finding of the short-range MCV6→RCH6 connectivity is less clear. The lower positive connectivity of the MCV6, which plays a major role in the automaticity process, with the RCH6 suggests that both of the cerebellar structures might complement one another in facilitating faster CS.

4.3. Negative causal influence in task-positive network

The few negative connectivities revealed in the interregional pairs of neural substrates, such as RMFC→LIPS and RMFC→RCV6, are somewhat counterintuitive under the context of a task-positive network. The main concern would be that temporal correlations of the neural substrates within a task-positive network should consistently be in positive values (Fox et al., 2005). Negative causal connectivity refers to a former neural substrate exerting negative influence on a latter neural substrate (Chen et al., 2011). When engaging in a task, better performance, such as shorter RTs, can be due to increases in effort or improvements in efficiency on task (Lin et al., 2011). It is noteworthy that increase in effort can be a consequence of stronger facilitative or inhibitory effects to be exerted from a former neural substrate functionally connecting to a latter neural substrate. For instance, our results showed higher negative connectivity of RMFC→LIPS predicted faster performance. Increases in BOLD signals of RMFC would have intensified the inhibitory effect on LIPS for producing shorter RTs. It is plausible that negative connectivities in a task-positive network should not be understood as suppression of task-relevant processes subserved by the network. It could be that the inhibitory effects of RMFC existed in the connective pairs, whereby playing a supervisory role accounted for the negative connectivity values. On the other hand, it could have been the increase in BOLD signals in the LIPS in response to the inhibition accounted for the positive values in the task-positive network. The explanations offered on the negative connectivities found in a task-positive network in this section need to be further verified in future study.

4.4. Limitations

This study has several limitations. First, there are ongoing debates on the application of Granger causality on fMRI (e.g., Barnett et al., 2018). One issue is the discrepancies in temporal resolutions of fMRI (i.e., 2 s) and those of neuronal activities (in sub-milliseconds). The shapes of hemodynamic responses also vary across different brain regions. Nevertheless, a previous study concluded that Granger causality analysis was found to adequately detect the causal influence (Seth et al., 2013), as the BOLD responses would have functioned as a low-pass filter, mitigating the low sampling frequency issue (Wen et al., 2013). When applied to effective connectivity analysis, other issues, such as vascular anatomy (Webb et al., 2013) and an over-parameterized model and interpretation of a signed path (Zhang et al., 2016), could have confounded the results. In particular, Webb et al. (2013) suggested that the blood flow in major cerebral arteries could introduce systematic BOLD signal latency across brain regions, leading to spurious “Granger-source” and “Granger-sink” brain regions. However, because the VAR model constructed in this study incorporated multiple ROIs, which also carried the vascular signals, the effect could have been mitigated, as the systematic BOLD latency could have been regressed out. Future studies should be conducted to justify our speculation. The current study revealed that the data-driven multivariate lagged model was superior to zero-lag correlation-based connectivity estimators in predicting PSs. Future studies should be conducted to test the replicability of the results and the application of the Granger-like path estimator to other constructs. Second, the task-negative network was not included in the current study because of the limited number of ROIs entered into the model to avoid overfitting of the multivariate connectivity estimation models. Previous studies demonstrated that the default-mode network was associated with slowed attentional RT (Weissman et al., 2006). Further study would extend the coverage of additional functional networks for building the PS model. Third, the two-modality and three-task rule design somewhat limited the option of establishing external validity of the results with those derived from public datasets. Future studies should employ different tasks but a similar design to test the reproducibility of the results. Fourth, the sample size was rather small, which could have weakened the power of the analyses. Readers should be cautious when interpreting the results. Finally, the CS was derived by regressing out the RTs of control conditions from those of experimental conditions. The former could have included the sensorimotor and decision-making components (Ratcliff and Van Dongen, 2011). Although the decisions made in the control conditions were relatively simple, it is not known how much the time involved would have impacted the CS. Future research could validate the merit of the partial method.

5. Conclusion

The findings of this study indicate that facilitative and inhibitory processes, which were shown to be subserved by a cerebello-frontal network, within a predefined set of regions, influenced cognitive processing speed. The effective connectivity analysis suggested that the RMFC and LCH6 were the core substrates that regulated the information process through task-set maintenance, and the LIFJ, LIPS and RCH6 were involved in the stream of stimulus-response information processing. The new findings on the antagonistic and agonistic roles among the cerebellar regions in cognitive processing speed require further investigation.

Declaration of Competing Interest

The authors declares that there is no conflict of interest regarding the publication of this article.

Credit authorship contribution statement

Clive H.Y. Wong: Conceptualization, Formal analysis, Investigation, Methodology, Software, Writing - original draft, Writing - review & editing. **Jiao Liu:** Conceptualization, Data curation, Investigation, Project administration, Writing - original draft, Writing - review & editing. **Tatia M.C. Lee:** Conceptualization, Funding acquisition, Resources, Supervision, Writing - review & editing. **Jing Tao:** Funding acquisition, Project administration, Resources, Supervision, Writing - review & editing. **Alex W.K. Wong:** Methodology, Writing - review & editing. **Bolton K.H. Chau:** Supervision, Writing - review & editing. **Lidian Chen:** Funding acquisition, Resources, Supervision, Writing - review & editing. **Chetwyn C.H. Chan:** Conceptualization, Supervision, Validation, Writing - original draft, Writing - review & editing.

Data and code availability

The ICA-cleaned imaging dataset, ANTs high-dimensional deformation and scripts for applying the deformation, cluster masks obtaioned with watershed method, and the extracted timeseries for all subjects are available in GitHub (https://github.com/clivehywong/2021CPS).

The processing speed tasks activation maps were obtained from NeuroVault (https://identifiers.org/neurovault.collection:857).

Watershed-based parcellation of activation map is available from https://www.med.upenn.edu/cmroi/shed.html.

Vector Autoregression connectivity indices were estimated with 1dGC (https://afni.nimh.nih.gov/1dgc).

The R scripts for estimating other connectivity indices and the mixed effect modeling are available in GitHub (https://github.com/clivehywong/2021CPS).

Acknowledgments

This study was supported by the 12th Five-year Plan project of Ministry of Science and Technology of the People's Republic of China (grant number 2013BAI10B01) and the Fujian Rehabilitation Tech Co-Innovation of China. It was also supported by The University of Hong Kong May Endowed Professorship in Neuropsychology and The Science and Technology Program of Guangdong (2018B030334001). The authors thank the University Research Facility in Behavioral and Systems Neuroscience, The Hong Kong Polytechnic University for the equipment and technical supports rendered throughout the study.

Supplementary materials

Supplementary material associated with this article can be found, in the online version, at doi:10.1016/j.neuroimage.2020.117556.

References

Akbar, N., Banwell, B., Sled, J.G., Binns, M.A., Doesburg, S.M., Rypma, B., et al., 2016. Brain activation patterns and cognitive processing speed in patients with pediatric-onset multiple sclerosis. J. Clin. Exp. Neuropsychol. 38 (4), 393–403. http://doi.org/10.1080/13803395.2015.1119255.

Argyropoulos, G.P., Kimiskidis, V.K., Papagiannopoulos, S., 2011. θ-burst stimulation of the right neocerebellar vermis selectively disrupts the practice-induced acceleration of lexical decisions. Behav. Neurosci. 125 (5), 724–734. http://doi.org/10.1037/a0025134.

Arslan, S., Ktena, S.I., Makropoulos, A., Robinson, E.C., Rueckert, D., Parisot, S., 2018. Human brain mapping: a systematic comparison of parcellation methods for the human cerebral cortex. Neuroimage 170, 5–30. http://doi.org/10.1016/j.neuroimage.2017.04.014.

Avants, B.B., Epstein, C.L., Grossman, M., Gee, J.C., 2008. Symmetric diffeomorphic image registration with cross-correlation: evaluating automated labeling of elderly and neurodegenerative brain. Med. Image Anal. 12 (1), 26–41. http://doi.org/10.1016/j.media.2007.06.004.

Avants, B.B., Tustison, N.J., Stauffer, M., Song, G., Wu, B., Gee, J.C., 2014. The Insight ToolKit image registration framework. Front. Neuroinform. 8 (52), 773. http://doi.org/10.3389/fninf.2014.00044.

Balsters, J.H., Ramnani, N., 2011. Cerebellar plasticity and the automation of first-order rules. J. Neurosci. 31 (6), 2305–2312. http://doi.org/10.1523/JNEUROSCI.4358-10.2011.

Barber, A.D., Carter, C.S., 2004. Cognitive control involved in overcoming prepotent response tendencies and switching between tasks. Cereb. Cortex 15 (7), 899–912. http://doi.org/10.1093/cercor/bhh189.

Barnett, L., Barrett, A.B., Seth, A.K., 2018. Solved problems for Granger causality in neuroscience: A response to Stokes and Purdon. NeuroImage 178, 744–748. doi:10.1016/j.neuroimage.2018.05.067.

Bates, T., Stough, C., 1998. Improved reaction time method, information processing speed, and intelligence. Intelligence 26 (1), 53–62. http://doi.org/10.1016/s0160-2896(99)80052-x.

Bernard, J.A., Seidler, R.D., 2013. Cerebellar contributions to visuomotor adaptation and motor sequence learning: an ALE meta-analysis. Front Hum Neurosci 7, 27. http://doi.org/10.3389/fnhum.2013.00027.

Binder, J.R., Liebenthal, E., Possing, E.T., Medler, D.A., Ward, B.D., 2004. Neural correlates of sensory and decision processes in auditory object identification. Nat. Neurosci. 7 (3), 295–301. http://doi.org/10.1038/nn1198.

Bisecco, A., Stamenova, S., Caiazzo, G., d'Ambrosio, A., Sacco, R., Docimo, R., et al., 2017. Attention and processing speed performance in multiple sclerosis is mostly related to thalamic volume. Brain Imaging Behav 12 (1), 20–28. http://doi.org/10.1007/s11682-016-9667-6.

Biswal, B.B., Eldreth, D.A., Motes, M.A., Rypma, B., 2010. Task-dependent individual differences in prefrontal connectivity. Cereb. Cortex 20 (9), 2188–2197. http://doi.org/10.1093/cercor/bhp284.

Buckner, R.L., Krienen, F.M., Castellanos, A., Diaz, J.C., Yeo, B.T.T., 2011. The organization of the human cerebellum estimated by intrinsic functional connectivity. J. Neurophysiol. 106 (5), 2322–2345. http://doi.org/10.1152/jn.00339.2011.

Chen, G., Glen, D.R., Saad, Z.S., Hamilton, J.P., Thomason, M.E., Gotlib, I.H., Cox, R.W., 2011. Vector autoregression, structural equation modeling, and their synthesis in neuroimaging data analysis. Comput. Biol. Med. 41 (12), 1142–1155. http://doi.org/10.1016/j.compbiomed.2011.09.004.

Clark, S.V., King, T.Z., Turner, J.A., 2020. Cerebellar contributions to proactive and reactive control in the stop signal task: a systematic review and meta-analysis of functional magnetic resonance imaging studies. Neuropsychol. Rev. 51 (4), 356. –24 http://doi.org/10.1007/s11065-020-09432-w .

Corbetta, M., Shulman, G.L., 2002. Control of goal-directed and stimulus-driven attention in the brain. Nat. Rev. Neurosci. 3 (3), 201–215. http://doi.org/10.1038/nrn755.

Deshpande, G., Sathian, K., Hu, X., 2010. Effect of hemodynamic variability on Granger causality analysis of fMRI. Neuroimage 52 (3), 884–896. http://doi.org/10.1016/j.neuroimage.2009.11.060.

Ding, H., Qin, W., Jiang, T., Zhang, Y., Yu, C., 2012. Volumetric variation in subregions of the cerebellum correlates with working memory performance. Neurosci. Lett. 508 (1), 47–51. http://doi.org/10.1016/j.neulet.2011.12.016.

Dosenbach, N.U.F., Visscher, K.M., Palmer, E.D., Miezin, F.M., Wenger, K.K., Kang, H.C., et al., 2006. A core system for the implementation of task sets. Neuron 50 (5), 799–812. http://doi.org/10.1016/j.neuron.2006.04.031.

D'Mello, A.M., Gabrieli, J.D.E., Nee, D.E., 2020. Evidence for hierarchical cognitive control in the human cerebellum. Curr. Biol. 30 (10), 1881–1892. http://doi.org/10.1016/j.cub.2020.03.028.

Eckert, M.A., 2011. Slowing down: age-related neurobiological predictors of processing speed. Front. Neurosci. 5, 25. http://doi.org/10.3389/fnins.2011.00025.

Eckert, M.A., Keren, N.I., Roberts, D.R., Calhoun, V.D., Harris, K.C., 2010. Age-related changes in processing speed: unique contributions of cerebellar and prefrontal cortex. Front. Hum. Neurosci. 4, 10. http://doi.org/10.3389/neuro.09.010.2010.

Esterman, M., Thai, M., Okabe, H., DeGutis, J., Saad, E., Laganiere, S.E., Halko, M.A., 2017. Network-targeted cerebellar transcranial magnetic stimulation improves attentional control. Neuroimage 156, 190–198. http://doi.org/10.1016/j.neuroimage.2017.05.011.

Fan, J., 2014. An information theory account of cognitive control. Front Hum Neurosci 8 (598), 680. http://doi.org/10.3389/fnhum.2014.00680.

Forn, C., Belloch, V., Bustamante, J.C., Garbin, G., Parcet-Ibars, M.À., Sanjuan, A., et al., 2009. A symbol digit modalities test version suitable for functional MRI studies. Neurosci. Lett. 456 (1), 11–14. http://doi.org/10.1016/j.neulet.2009.03.081.

Forn, C., Ripollés, P., Cruz-Gómez, A.J., Belenguer, A., González-Torre, J.A., Ávila, C., 2013. Task-load manipulation in the Symbol Digit Modalities Test: an alternative measure of information processing speed. Brain Cogn. 82 (2), 152–160. http://doi.org/10.1016/j.bandc.2013.04.003.

Fox, M.D., Snyder, A.Z., Vincent, J.L., Corbetta, M., Van Essen, D.C., Raichle, M.E., 2005. The human brain is intrinsically organized into dynamic, anticorrelated functional networks. Proc. Natl. Acad. Sci. 102 (27), 9673–9678. http://doi.org/10.1073/pnas.0504136102.

Frank, E., Prien, R.F., Jarrett, R.B., Keller, M.B., Kupfer, D.J., Lavori, P.W., et al., 1991. Conceptualization and rationale for consensus definitions of terms in major depressive disorder. Remission, recovery, relapse, and recurrence. Arch. Gen. Psychiatry 48 (9), 851–855.

Gao, M., Wong, C.H.Y., Huang, H., Shao, R., Huang, R., Chan, C.C.H., Lee, T.M.C., 2020. Connectome-based models can predict processing speed in older adults. Neuroimage 223, 117290. http://doi.org/10.1016/j.neuroimage.2020.117290.

Genova, H.M., Hillary, F.G., Wylie, G., Rypma, B., DeLuca, J., 2009. Examination of processing speed deficits in multiple sclerosis using functional magnetic resonance imaging. J. Int. Neuropsychol. Soc. 15 (3), 383–393. http://doi.org/10.1017/S1355617709090535.

Groll, A., Tutz, G., 2014. Variable selection for generalized linear mixed models by L 1-penalized estimation. Stat. Comput. 24 (2), 137–154. http://doi.org/10.1007/s11222-012-9359-z.

Guillery, R.W., Sherman, S.M., 2002. Thalamic relay functions and their role in corticocortical communication: generalizations from the visual system. Neuron 33 (2), 163–175. http://doi.org/10.1016/s0896-6273(01)00582-7.

Habas, C., Kamdar, N., Nguyen, D., Prater, K., Beckmann, C.F., Menon, V., Greicius, M.D., 2009. Distinct cerebellar contributions to intrinsic connectivity networks. J. Neurosci. 29 (26), 8586–8594. http://doi.org/10.1523/JNEUROSCI.1868-09.2009.

Habeck, C.G., Gazes, Y., Razlighi, Q., Steffener, J., Brickman, A., Barulli, D., et al., 2016. The Reference Ability Neural Network Study: life-time stability of reference-ability neural networks derived from task maps of young adults. Neuroimage 125, 693–704. http://doi.org/10.1016/j.neuroimage.2015.10.077.

Hahn, B., Ross, T.J., Stein, E.A., 2007. Cingulate activation increases dynamically with response speed under stimulus unpredictability. Cereb. Cortex 17 (7), 1664–1671. http://doi.org/10.1093/cercor/bhl075.

Harding, I.H., Yücel, M., Harrison, B.J., Pantelis, C., Breakspear, M., 2015. Effective connectivity within the frontoparietal control network differentiates cognitive control and working memory. Neuroimage 106, 144–153. http://doi.org/10.1016/j.neuroimage.2014.11.039.

Hu, S., Ide, J.S., Zhang, S., Li, C.-S.R., 2016. The right superior frontal gyrus and individual variation in proactive control of impulsive response. J. Neurosci. 36 (50), 12688–12696. http://doi.org/10.1523/JNEUROSCI.1175-16.2016.

Hu, S., Tseng, Y.-C., Winkler, A.D., Li, C.-S.R., 2014. Neural bases of individual variation in decision time. Hum. Brain Mapp. 35 (6), 2531–2542. http://doi.org/10.1002/hbm.22347.

Jenkinson, M., Beckmann, C.F., Behrens, T.E.J., Woolrich, M.W., Smith, S.M., 2012. FSL. Neuroimage 62 (2), 782–790. http://doi.org/10.1016/j.neuroimage.2011.09.015.

Jensen, A.R. (2006). Clocking the Mind. Elsevier. http://doi.org/10.1111/j.1744-6570.2008.00111_7.x

Jensen, A.R., Reed, T.E., 1990. Simple reaction time as a suppressor variable in the chronometric study of intelligence. Intelligence 14 (4), 375–388. http://doi.org/10.1016/s0160-2896(05)80011-x.

Kansal, K., Yang, Z., Fishman, A.M., Sair, H.I., Ying, S.H., Jedynak, B.M., et al., 2017. Structural cerebellar correlates of cognitive and motor dysfunctions in cerebellar degeneration. Brain 140 (3), 707–720. http://doi.org/10.1093/brain/aww327.

Kellermann, T., Regenbogen, C., De Vos, M., Mößnang, C., Finkelmeyer, A., Habel, U., 2012. Effective connectivity of the human cerebellum during visual attention. J. Neurosci. 32 (33), 11453–11460. http://doi.org/10.1523/JNEUROSCI.0678-12.2012.

Kelly, R.E., Alexopoulos, G.S., Wang, Z., Gunning, F.M., Murphy, C.F., Morimoto, S.S., et al., 2010. Visual inspection of independent components: defining a procedure for artifact removal from fMRI data. J. Neurosci. Methods 189 (2), 233–245. http://doi.org/10.1016/j.jneumeth.2010.03.028.

Klein, A., Andersson, J., Ardekani, B.A., Ashburner, J., Avants, B., Chiang, M.-.C., et al., 2009. Evaluation of 14 nonlinear deformation algorithms applied to human brain MRI registration. Neuroimage 46 (3), 786–802. http://doi.org/10.1016/j.neuroimage.2008.12.037.

Korb, F.M., Jiang, J., King, J.A., Egner, T., 2017. Hierarchically organized medial frontal cortex-basal ganglia loops selectively control task- and response-selection. J. Neurosci. 37 (33), 7893–7905. http://doi.org/10.1523/JNEUROSCI.3289-16.2017.

la Vega, de, A., Chang, L.J., Banich, M.T., Wager, T.D., Yarkoni, T., 2016. Large-scale meta-analysis of human medial frontal cortex reveals tripartite functional organization. J. Neurosci. 36 (24), 6553–6562. http://doi.org/10.1523/JNEUROSCI.4402-15.2016.

Langner, R., Eickhoff, S.B., 2013. Sustaining attention to simple tasks: a meta-analytic review of the neural mechanisms of vigilant attention. Psychol. Bull. 139 (4), 870–900. http://doi.org/10.1037/a0030694.

Lee, T.M.C., Zhang, J.X., Chan, C.C.H., Yuen, K.S.L., Chu, L.W., Cheung, R.T.F., et al., 2006. Age-related differences in response regulation as revealed by functional MRI. Brain Res. 1076 (1), 171–176. http://doi.org/10.1016/j.brainres.2005.12.124.

Lee, T.M.C., Zhou, W.-.H., Luo, X.-.J., Yuen, K.S.L., Ruan, X.-.Z., Weng, X.-.C., 2005. Neural activity associated with cognitive regulation in heroin users: a fMRI study. Neurosci. Lett. 382 (3), 211–216. http://doi.org/10.1016/j.neulet.2005.03.053.

Lin, F.-.H., Agnew, J.A., Belliveau, J.W., Zeffiro, T.A., 2009. Functional and effective connectivity of visuomotor control systems demonstrated using generalized partial least squares and structural equation modeling. Hum. Brain Mapp. 30 (7), 2232–2251. http://doi.org/10.1002/hbm.20664.

Lin, P., Hasson, U., Jovicich, J., Robinson, S., 2011. A neuronal basis for task-negative responses in the human brain. Cereb. Cortex 21 (4), 821–830. http://doi.org/10.1093/cercor/bhq151.

Liu, Z., Braunlich, K., Wehe, H.S., Seger, C.A., 2015. Neural networks supporting switching, hypothesis testing, and rule application. Neuropsychologia 77, 19–34. http://doi.org/10.1016/j.neuropsychologia.2015.07.019.

Luis, E.O., Arrondo, G., Vidorreta, M., Martínez, M., Loayza, F., Fernández-Seara, M.A., Pastor, M.A., 2015. Successful working memory processes and cerebellum in an elderly sample: a neuropsychological and fMRI study. PLoS ONE 10 (7), e0131536. http://doi.org/10.1371/journal.pone.0131536.

Madden, D.J., Spaniol, J., Whiting, W.L., Bucur, B., Provenzale, J.M., Cabeza, R.E., et al., 2007. Adult age differences in the functional neuroanatomy of visual attention: a combined fMRI and DTI study. Neurobiol. Aging 28 (3), 459–476. http://doi.org/10.1016/j.neurobiolaging.2006.01.005.

Mawase, F., Bar-Haim, S., Shmuelof, L., 2017. Formation of long-term locomotor memories is associated with functional connectivity changes in the cerebellar-thalamic-cortical network. J. Neurosci. 37 (2), 349–361. http://doi.org/10.1523/JNEUROSCI.2733-16.2016.

Mayr, U., Diedrichsen, J., Ivry, R., Keele, S.W., 2006. Dissociating task-set selection from task-set inhibition in the prefrontal cortex. J. Cogn. Neurosci. 18 (1), 14–21. http://doi.org/10.1162/089892906775250085.

Motes, M.A., Biswal, B.B., Rypma, B., 2011. Age-dependent relationships between prefrontal cortex activation and processing efficiency. Cogn. Neurosci. 2 (1), 1–10. http://doi.org/10.1080/17588928.2010.512974.

Murray, M.M., Wallace, M.T., Cappe, C., Rouiller, E.M., & Barone, P. (2012). Cortical and thalamic pathways for multisensory and sensorimotor interplay.

Naito, E., Kinomura, S., Geyer, S., Kawashima, R., Roland, P.E., Zilles, K., 2000. Fast reaction to different sensory modalities activates common fields in the motor areas, but the anterior cingulate cortex is involved in the speed of reaction. J. Neurophysiol. 83 (3), 1701–1709.

Nakagawa, S., Schielzeth, H., 2012. A general and simple method for obtaining R2 from generalized linear mixed-effects models. Methods Ecol. Evol. 4 (2), 133–142. http://doi.org/10.1111/j.2041-210x.2012.00261.x.

O'Reilly, J.X., Mesulam, M.-.M., Nobre, A.C., 2008. The cerebellum predicts the timing of perceptual events. J. Neurosci. 28 (9), 2252–2260. http://doi.org/10.1523/JNEUROSCI.2742-07.2008.

Oldfield, R.C., 1971. The assessment and analysis of handedness: the Edinburgh inventory. Neuropsychologia 9 (1), 97–113. http://doi.org/10.1016/0028-3932(71)90067-4.

Paul, R., Grieve, S.M., Chaudary, B., Gordon, N., Lawrence, J., Cooper, N., et al., 2009. Relative contributions of the cerebellar vermis and prefrontal lobe volumes on cognitive function across the adult lifespan. Neurobiol. Aging 30 (3), 457–465. http://doi.org/10.1016/j.neurobiolaging.2007.07.017.

Pfaff, B., 2008. VAR, SVAR and SVEC models: implementation within R package vars. J. Stat. Softw. 27 (4). http://doi.org/10.18637/jss.v027.i04.

Prevosto, V., Sommer, M.A., 2013. Cognitive control of movement via the cerebellar-recipient thalamus. Front. Syst. Neurosci. 7, 56. http://doi.org/10.3389/fnsys.2013.00056.

Ramnani, N., 2014. Automatic and controlled processing in the corticocerebellar system. Prog. Brain Res. 210, 255–285. http://doi.org/10.1016/B978-0-444-63356-9.00010-8.

Ratcliff, R., Van Dongen, H.P.A., 2011. Diffusion model for one-choice reaction-time tasks and the cognitive effects of sleep deprivation. Proc. Natl. Acad. Sci. 108 (27), 11285–11290. http://doi.org/10.1073/pnas.1100483108.

Razlighi, Q.R., Habeck, C.G., Barulli, D., Stern, Y., 2017. Cognitive neuroscience neuroimaging repository for the adult lifespan. Neuroimage 144 (Pt B), 294–298. http://doi.org/10.1016/j.neuroimage.2015.08.037.

Reid, A.T., Headley, D.B., Mill, R.D., Sanchez-Romero, R., Uddin, L.Q., Marinazzo, D., et al., 2019. Advancing functional connectivity research from association to causation. Nat. Neurosci. 22 (11), 1751–1760. http://doi.org/10.1038/s41593-019-0510-4.

Reineberg, A.E., Banich, M.T., 2016. Functional connectivity at rest is sensitive to individual differences in executive function: a network analysis. Hum. Brain Mapp.. http://doi.org/10.1002/hbm.23219.

Roberts, R.D., Stankov, L., 1999. Individual differences in speed of mental processing and human cognitive abilities: toward a taxonomic model. Learn. Individ. Differ. 11 (1), 1–120. http://doi.org/10.1016/S1041-6080(00)80007-2.

Roth, A.K., Denney, D.R., Lynch, S.G., 2015. Information processing speed and attention in multiple sclerosis: reconsidering the Attention Network Test (ANT). J. Clin. Exp. Neuropsychol. 37 (5), 518–529. http://doi.org/10.1080/13803395.2015.1037252.

Ruet, A., Hamel, D., Deloire, M.S.A., Charré-Morin, J., Saubusse, A., Brochet, B., 2014. Information processing speed impairment and cerebellar dysfunction in relapsing-remitting multiple sclerosis. J. Neurol. Sci. 347 (1–2), 246–250. http://doi.org/10.1016/j.jns.2014.10.008.

Rypma, B., Berger, J.S., Prabhakaran, V., Bly, B.M., Kimberg, D.Y., Biswal, B.B., D'Esposito, M., 2006. Neural correlates of cognitive efficiency. Neuroimage 33 (3), 969–979. http://doi.org/10.1016/j.neuroimage.2006.05.065.

Salmi, J., Pallesen, K.J., Neuvonen, T., Brattico, E., Korvenoja, A., Salonen, O., Carlson, S., 2010. Cognitive and motor loops of the human cerebro-cerebellar system. J. Cogn. Neurosci. 22 (11), 2663–2676. http://doi.org/10.1162/jocn.2009.21382.

Salmi, J., Rinne, T., Koistinen, S., Salonen, O., Alho, K., 2009. Brain networks of bottom-up triggered and top-down controlled shifting of auditory attention. Brain Res. 1286, 155–164. http://doi.org/10.1016/j.brainres.2009.06.083.

Sanchez-Romero, R., Cole, M.W., 2020. Combining multiple functional connectivity methods to improve causal inferences. J. Cogn. Neurosci. 3, 1–15. http://doi.org/10.1162/jocn_a_01580.

Satterthwaite, T.D., Wolf, D.H., Erus, G., Ruparel, K., Elliott, M.A., Gennatas, E.D., et al., 2013. Functional maturation of the executive system during adolescence. J. Neurosci. 33 (41), 16249–16261. http://doi.org/10.1523/JNEUROSCI.2345-13.2013.

Selya, A.S., Rose, J.S., Dierker, L.C., Hedeker, D., Mermelstein, R.J., 2012. A Practical Guide to Calculating Cohen's f(2), a measure of local effect size, from PROC MIXED. Front Psychol 3, 111. http://doi.org/10.3389/fpsyg.2012.00111.

Seth, A.K., Chorley, P., Barnett, L.C., 2013. Granger causality analysis of fMRI BOLD signals is invariant to hemodynamic convolution but not downsampling. Neuroimage 65, 540–555. http://doi.org/10.1016/j.neuroimage.2012.09.049.

Shine, J.M., Shine, R., 2014. Delegation to automaticity: the driving force for cognitive evolution? Front Neurosci 8 (116), 90. http://doi.org/10.3389/fnins.2014.00090.

Shulman, G.L., Astafiev, S.V., Franke, D., Pope, D.L.W., Snyder, A.Z., McAvoy, M.P., Corbetta, M., 2009. Interaction of stimulus-driven reorienting and expectation in ventral and dorsal frontoparietal and basal ganglia-cortical networks. J. Neurosci. 29 (14), 4392–4407. http://doi.org/10.1523/JNEUROSCI.5609-08.2009.

Silva, P.H.R., Spedo, C.T., Baldassarini, C.R., Benini, C.D., Ferreira, D.A., Barreira, A.A., Leoni, R.F., 2019. Brain functional and effective connectivity underlying the information processing speed assessed by the Symbol Digit Modalities Test. Neuroimage 184, 761–770. http://doi.org/10.1016/j.neuroimage.2018.09.080.

Smith, S.M., Miller, K.L., Salimi-Khorshidi, G., Webster, M., Beckmann, C.F., Nichols, T.E., et al., 2011. Network modelling methods for FMRI. Neuroimage 54 (2), 875–891. http://doi.org/10.1016/j.neuroimage.2010.08.063.

Spagna, A., Mackie, M.-.A., Fan, J., 2015. Supramodal executive control of attention. Front. Psychol. 6 (680), 65. http://doi.org/10.3389/fpsyg.2015.00065.

Stoodley, C.J., Valera, E.M., Schmahmann, J.D., 2012. Functional topography of the cerebellum for motor and cognitive tasks: an fMRI study. Neuroimage 59 (2), 1560–1570. http://doi.org/10.1016/j.neuroimage.2011.08.065.

Sweet, L.H., Paskavitz, J.F., O'Connor, M.J., Browndyke, J.N., Wellen, J.W., Cohen, R.A., 2005. FMRI correlates of the WAIS-III symbol search subtest. J. Int. Neuropsychol. Soc. 11 (4), 471–476. http://doi.org/10.1017/s1355617705050575.

Takeuchi, H., Kawashima, R., 2012. Effects of processing speed training on cognitive functions and neural systems. Rev. Neurosci. 23 (3), 289–301. http://doi.org/10.1515/revneuro-2012-0035.

Tamber-Rosenau, B.J., Dux, P.E., Tombu, M.N., Asplund, C.L., Marois, R., 2013. Amodal processing in human prefrontal cortex. J. Neurosci. 33 (28), 11573–11587. http://doi.org/10.1523/JNEUROSCI.4601-12.2013.

Tark, K.-.J., Curtis, C.E., 2009. Persistent neural activity in the human frontal cortex when maintaining space that is off the map. Nat. Neurosci. 12 (11), 1463–1468. http://doi.org/10.1038/nn.2406.

Tunik, E., Rice, N.J., Hamilton, A., Grafton, S.T., 2007. Beyond grasping: representation of action in human anterior intraparietal sulcus. Neuroimage 36 (Suppl 2), T77–T86. http://doi.org/10.1016/j.neuroimage.2007.03.026.

Verhaeghen, P., 2011. Aging and executive control: reports of a demise greatly exaggerated. Curr. Dir. Psychol. Sci. 20 (3), 174–180. http://doi.org/10.1177/0963721411408772.

Waiter, G.D., Fox, H.C., Murray, A.D., Starr, J.M., Staff, R.T., Bourne, V.J., et al., 2008. Is retaining the youthful functional anatomy underlying speed of information processing a signature of successful cognitive ageing? An event-related fMRI study of inspection time performance. Neuroimage 41 (2), 581–595. http://doi.org/10.1016/j.neuroimage.2008.02.045.

Webb, J.T., Ferguson, M.A., Nielsen, J.A., Anderson, J.S., 2013. BOLD granger causality reflects vascular anatomy. PLoS ONE 8 (12), e84279. http://doi.org/10.1371/journal.pone.0084279.

Wechsler, D., 1981. WAIS-R, Wechsler Adult Intelligence Scale- Revised, Manual.

Weissman, D.H., Roberts, K.C., Visscher, K.M., Woldorff, M.G., 2006. The neural bases of momentary lapses in attention. Nat. Neurosci. 9 (7), 971–978. http://doi.org/10.1038/nn1727.

Wen, X., Rangarajan, G., Ding, M., 2013. Is Granger causality a viable technique for analyzing fMRI data? PLoS ONE 8 (7), e67428. http://doi.org/10.1371/journal.pone.0067428.

Woodward, N.D., Duffy, B., Karbasforoushan, H., 2013. Prefrontal cortex activity during response selection predicts processing speed impairment in schizophrenia. J. Int. Neuropsychol. Soc. 19 (7), 782–791. http://doi.org/10.1017/S1355617713000532.

Woolgar, A., Thompson, R., Bor, D., Duncan, J., 2011. Multi-voxel coding of stimuli, rules, and responses in human frontoparietal cortex. Neuroimage 56 (2), 744–752. http://doi.org/10.1016/j.neuroimage.2010.04.035.

Yu, J., Li, J., Huang, X., 2012. The Beijing version of the montreal cognitive assessment as a brief screening tool for mild cognitive impairment: a community-based study. BMC Psychiatry 12 (1), 156. http://doi.org/10.1186/1471-244X-12-156.

Zhang, H., Eppes, A., Beatty-Martínez, A., Navarro-Torres, C., Diaz, M.T., 2018. Task difficulty modulates brain-behavior correlations in language production and cognitive control: behavioral and fMRI evidence from a phonological go/no-go picture-naming paradigm. Cognit. Affect. Behav. Neurosci. 18 (5), 964–981. http://doi.org/10.3758/s13415-018-0616-2.

Zhang, J., Li, C., Jiang, T., 2016. New insights into signed path coefficient granger causality analysis. Front. Neuroinform. 10, 47. http://doi.org/10.3389/fninf.2016.00047.